Journal of Asian Earth Sciences 35 (2009) 310–322

Contents lists available at ScienceDirect

Journal of Asian Earth Sciences

journal homepage: www.elsevier.com/locate/jaes

UHP metamorphic evolution and SHRIMP geochronology of a coesite-bearing meta-ophiolitic gabbro in the North Qaidam, NW China

Guibin Zhang [a], Lifei Zhang [a,*], Shuguang Song [a], Yaoling Niu [b]

[a] MOE Key Laboratory of Orogenic Belts and Crustal Evolution, School of Earth and Space Sciences, Peking University, Beijing 100871, China
[b] Department of Earth Science, Durham University, Durham, DH1 3LE, UK

ARTICLE INFO

Article history:
Received 8 September 2008
Received in revised form 25 November 2008
Accepted 26 November 2008

Keywords:
Coesite inclusion
Eclogite
P-T path
SHRIMP dating of zircon
North Qaidam UHP belt
NW China

ABSTRACT

We have for the first-time observed the well-preserved coesite inclusions in a kyanite-eclogite from the Shaliuhe terrane of the North Qaidam ultra-high pressure (UHP) metamorphic belt, NW China. This provides convincing evidence for UHP metamorphism for the North Qaidam eclogite. Detailed petrography indicates that the kyanite-eclogite records complex metamorphic histories that can be broadly described in terms of three stages: (1) a pre-peak metamorphic stage characterized by the mineral assemblage of Grt + Amp + Pl + Qtz at P = 0.49–0.67 GPa and T = 410–490 °C; (2) a peak eclogite-facies stage with a mineral assemblage of Grt + Omp + Ky + Phn + Rt ± Qtz/Coe at P = 2.7–3.4 GPa and T = 610–700 °C; (3) a retrograde "stage" represented by reaction texture which includes the garnet reaction rims, the breakdown of omphacite, the symplectitic breakdown of kyanite, the retrograded garnet amphibolite assemblage and the latest greenschist-facies overprint. Zircon U–Pb SHRIMP dating shows the peak UHP metamorphic age of the kyanite-eclogite to be ~440 Ma. These data indicate that the kyanite-eclogite had ever been subducted to mantle depth of ~100 km in the end of the Ordovician. All these observations allow the construction of a P-T path for the kyanite-eclogite, suggesting a cold geothermal gradient and rapid subduction, ultimately followed by rapid exhumation in response to continental collision in Shaliuhe terrane and throughout the North Qaidam UHP metamorphic belt.

1. Introduction

The evolution of an orogenic belt generally involves in its early history, the subduction of oceanic/continental lithosphere into great depth, as documented in the Dabie-Sulu (Jahn, 1999; Liou and Zhang, 2002; Liou et al., 2004; Zheng et al., 2003) and West Tianshan mountain ranges (Zhang et al., 2002a, b, 2003 2007) in China, and the western Alpine orogenic belt (Reinecke, 1991; Bucher et al., 2005). The evidence for deep subduction, or ultra-high pressure (UHP) metamorphism, is often preserved in host rocks as rare mineral inclusions or relict mineral assemblages that can only be stable at high pressures (i.e. >2.5 GPa) (Mattinson et al., 2006).

The presence of coesite in zircons from paragneisses in the Dulan terrane (Yang et al., 2001; Song, 2001; Song et al., 2003a) established the North Qaidam UHP metamorphic belt, NW China. Although eclogites are volumetrically minor in UHP metamorphic terranes, they are the principal rocks that bear evidence of UHP metamorphism (Jahn et al., 2003). So far, only quartz exsolution in omphacite (Song et al., 2003a; Zhang et al., 2005b) and coesite pseudomorphs (Song et al., 2003a) have been documented for North Qaidam UHP eclogites.

In this paper, we report the first-time recognition of coesite in a Ky-eclogite of ophiolitic gabbro protolith from the Shaliuhe ophiolitic sequence (Zhang et al., 2008) in the North Qaidam UHP metamorphic belt, and discuss the detailed petrography and SHRIMP zircon geochronology of the coesite-bearing eclogites and their tectonic implications.

2. Geological background

The North Qaidam UHP metamorphic belt is located at the northern margin of the Tibetan Plateau (Fig. 1a); it extends NW–SE, and is bounded to the southwest by the Qaidam Block, and to the northeast by the Qilian Block (Fig. 1b). The Qaidam Block is a mesozoic intra-continental basin developed on the Precambrian crystalline basement. The Qilian Block comprises mainly Paleozoic sedimentary rocks underlain by an imbricate thrust belt of Precambrian basement, which consists of granitic gneiss, pelitic gneiss, schist and marble. The Altun HP/UHP rocks to the northwest are believed to be the northwestward extension of the North Qaidam UHP metamorphic belt (Fig. 1a) offset by the left-lateral Altyn Tagh fault zone (Liu et al., 1999; Zhang et al., 2001, 2005b; Mattinson et al., 2007). In the North Qaidam UHP metamorphic belt, eclogites

* Corresponding author.
E-mail address: Lfzhang@pku.edu.cn (L. Zhang).

1367-9120/$ - see front matter © 2008 Elsevier Ltd. All rights reserved.
doi:10.1016/j.jseaes.2008.11.013

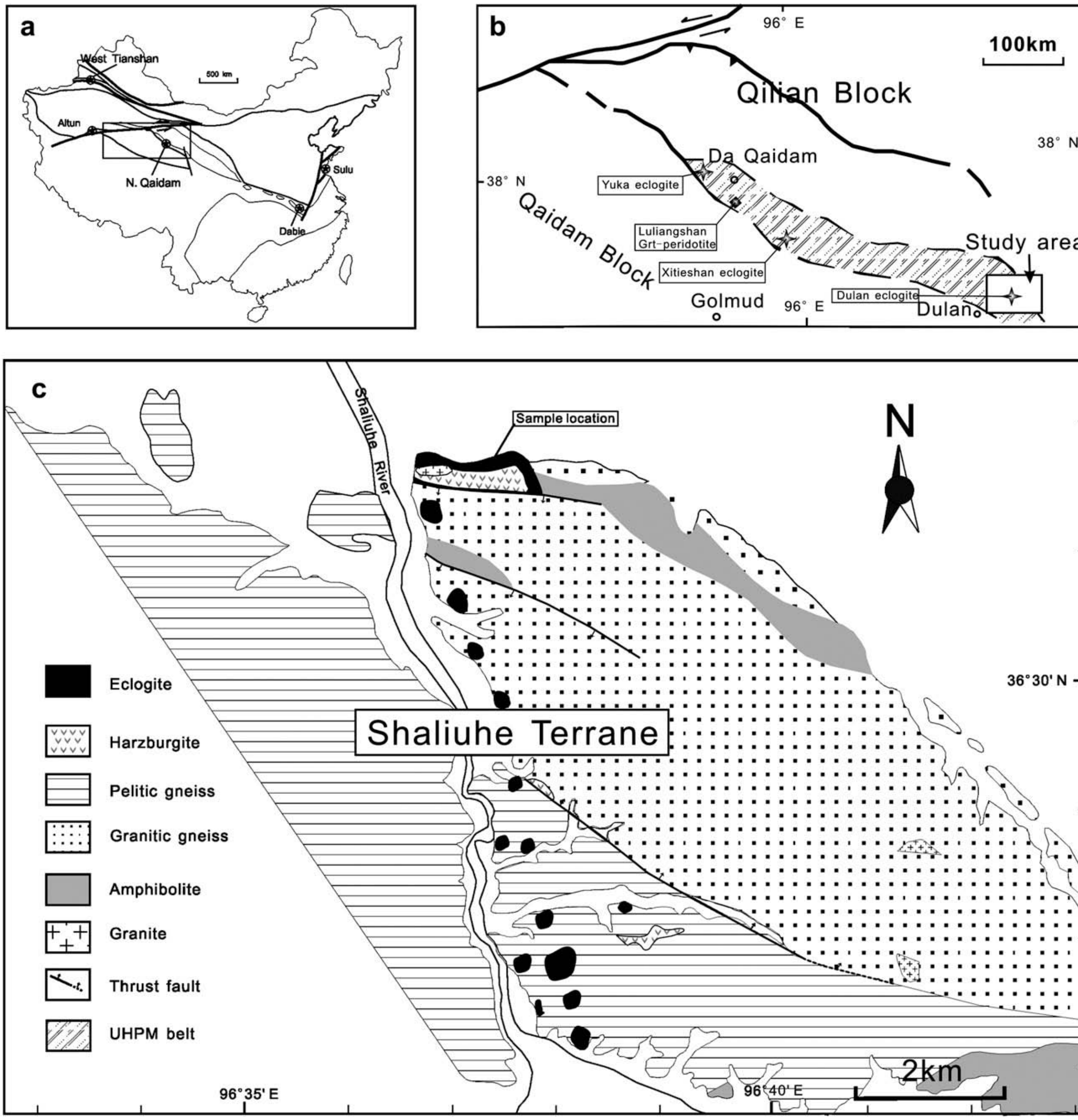

Fig. 1. Geological sketch map of the Shaliuhe UHP metamorphic terrane, North Qaidam UHPM belt, China (modified after Zhang et al., 2008).

are exposed in several localities (e.g. Yuka, Xitieshan, and Dulan) extending from northwest to southeast for about 400 km (Fig. 1b). A large block of garnet peridotite crops out at Luliangshan (Fig. 1b) (Yang and Deng, 1994), and has been suggested to exhume from mantle depths in excess of 200 km (Song et al., 2004, 2005a, b). The eclogite and peridotite occur as blocks or layers within the para- and ortho-gneisses in this UHP metamorphic belt.

The North Qaidam UHP metamorphic belt is interpreted as representing an Early Paleozoic continental collision zone (e.g. Song et al., 2005b, 2006). U/Pb dating of metamorphic zircons in eclogite from Yuka yields 488–495 Ma (TIMS and SHRIMP, Menold et al., 2002; Zhang et al., 2005b) and 430–440 Ma (LA-ICP-MS, Chen et al., 2007). Eclogite from Xitieshan gives similar UHP metamorphic age of $\sim$ 486 Ma (Zhang et al., 2005b). Song et al. (2003b, 2006) obtained $\sim$460 Ma for eclogite and $\sim$420 Ma for coesite-bearing zircons in paragneisses from the Dulan area using combined whole-rock Sm–Nd isochron and zircon U/Pb dating methods. Mattinson et al. (2006) suggested a $\sim$25 m.y. duration (422–449 Ma) of eclogite-facies metamorphism for the Dulan eclogite. The protolith age was reported to vary from the late Proterozoic to the early Ordovician based on eclogite samples from different locations along the belt (Zhang et al., 2005b; Yang et al., 2003; Zhang et al., 2008).

Our study area, the Shaliuhe terrane, is situated near Dulan at the eastern end of the North Qaidam UHP metamorphic belt (Fig. 1b), where eclogite and serpentinized harzburgite crop out (Fig. 1c). On the basis of mineral assemblage, three types of eclogite were recognized, i.e., kyanite (Ky) -eclogite, epidote (Ep) -eclogite and phengite (Phn) -eclogite. They occur either as lenses within granitic and pelitic gneisses or as interlayers with marbles (Zhang et al., 2008). The kyanite-eclogite, which we study here, was collected at the north end of this terrane (Fig. 1c). The kyanite-eclogite is a large lensoid block, about 800 m wide and 1700 m long (Fig. 1c), enclosing the serpentinized harzburgite (Fig. 2c). The kyanite-eclogite is geochemically characterized by the flat REE patter and distinct positive Eu anomaly, low TiO_2, high Al_2O_3 and MgO contents which implies the protolith of Ky-eclogite maybe the cumulate gabbro (Zhang et al., 2008). Field relations and above geochemical studies suggest that the kyanite-eclogite, the coexisting serpentinized harzburgite and the other two types of basaltic eclogite constitute an oceanic lithostratigraphic section of an ophiolitic sequence from mantle peridotite to cumulate and to upper basaltic rocks (Zhang et al., 2008). The country rocks are strongly mylonitized granitic gneisses (Fig. 2d).

3. Sample description

3.1. Kyanite-eclogite

The kyanite-eclogite shows a banded structure (Fig. 2a and b) defined by compositional bands of pink garnet-rich and green omphacite-rich layers. The layering may be inherited from the protolith (i.e. cumulate gabbro, Zhang et al., 2008). The garnet-rich layers contain more kyanite and finer-grained garnets (~3 mm) than the omphacite-rich layers. Garnets from the omphacite-rich layers are coarse porphyroblasts (about 5 mm and >10 mm for the largest grain), surrounded by omphacite and less kyanite (Fig. 3a). Kyanite, epidote, amphibole, plagioclase and quartz inclusions are preserved in garnet cores (Fig. 3b). Rare omphacitic clinopyroxene inclusions are present within garnet rims (Fig. 3b). These mineral inclusions record the growth history of garnet. Garnet grains in "altered" samples are commonly rimmed by kelyphite of green amphibole and plagioclase intergrowth (Fig. 3c).

Three generations of clinopyroxenes have been distinguished in the eclogite: (1) Cpx_1 occurs as inclusions in the garnet rim region (Fig. 3b) (mineral abbreviations after Kretz, 1983); (2) Cpx_2, the peak metamorphic omphacite, occurs as porphyroblasts making up ~40–45 vol.% of the rock matrix; and (3) Cpx_3, as a product of decompression breakdown of omphacite (i.e. Cpx + Pl symplectitic aggregates replaced by later Amp + Pl) (Fig. 3c). Quartz exsolution lamellae (~2–4 μm wide and ~50–200 μm long) are abundant in omphacite (Fig. 3d).

Kyanite is a major eclogitic peak stage mineral (Zhang et al., 2008). It occurs either as xenoblast (1–5 mm long, ~10–15 vol.% of the rock matrix) in equilibrium with garnet and omphacite, or as inclusions preserved in garnet and omphacite. Porphyroblastic kyanite is generally rimmed by a corona of plagioclase (Fig. 3f), or entirely replaced by very fine-grained symplectite of spinel in plagioclase (Fig. 3g).

Phengite occurs as a minor (<1 vol.%) phase associated with garnet porphyroblasts in the eclogite (Fig. 3b, e). Most phengite crystals have been replaced by a corona of Pl + Bt symplectite.

Garnet-amphibolite is retrogressed from eclogite; amphibole and plagioclase occur as neoblastic phases surrounding garnet (Fig. 3h); no omphacite relics are preserved. Margarite and zoisite occupy much of the kyanite pseudomorphs. In addition, minor rutile and quartz are also present.

From reaction textures and mineral assemblages of the kyanite-eclogite and highly retrogressed garnet-amphibolite, four stages of metamorphic recrystallization can be recognized at P-T conditions of the epidote-amphibolite, eclogite, amphibolite and greenschist-facies. Fresh kyanite-eclogite samples consist of peak stage assemblage of Grt (~40 vol.%) + Omp (~40 vol.%) + Ky (~15 vol.%) + Rt (<5 vol.%) ± Phn (Fig. 3a). Inclusions (Amp + Ep + Pl + Ky + Qtz) preserved in garnet interiors record a prograde growth history in the epidote-amphibolite facies (Fig. 3b). For the retrogression stage, omphacite developed initially Cpx + Pl symplectite (Fig. 3c). Garnet rims were replaced by a collar of kelyphitic amphibole and plagio-

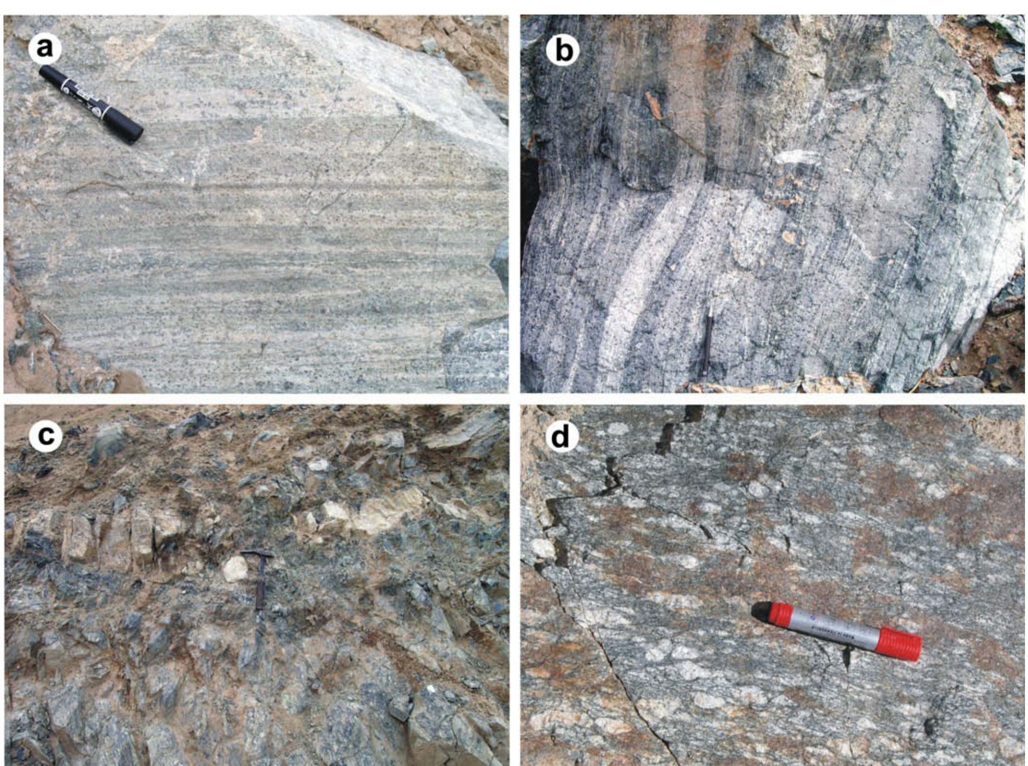

Fig. 2. Field view of kyanite-eclogite blocks and country rocks in the Shaliuhe terrane, North Qaidam UHPM belt, China. (a) and (b) showing banded structure of the kyanite-eclogite. (c) Serpentinized harzburgite enclosed within the kyanite-eclogite. (d) The granitic gneiss that host the eclogite.

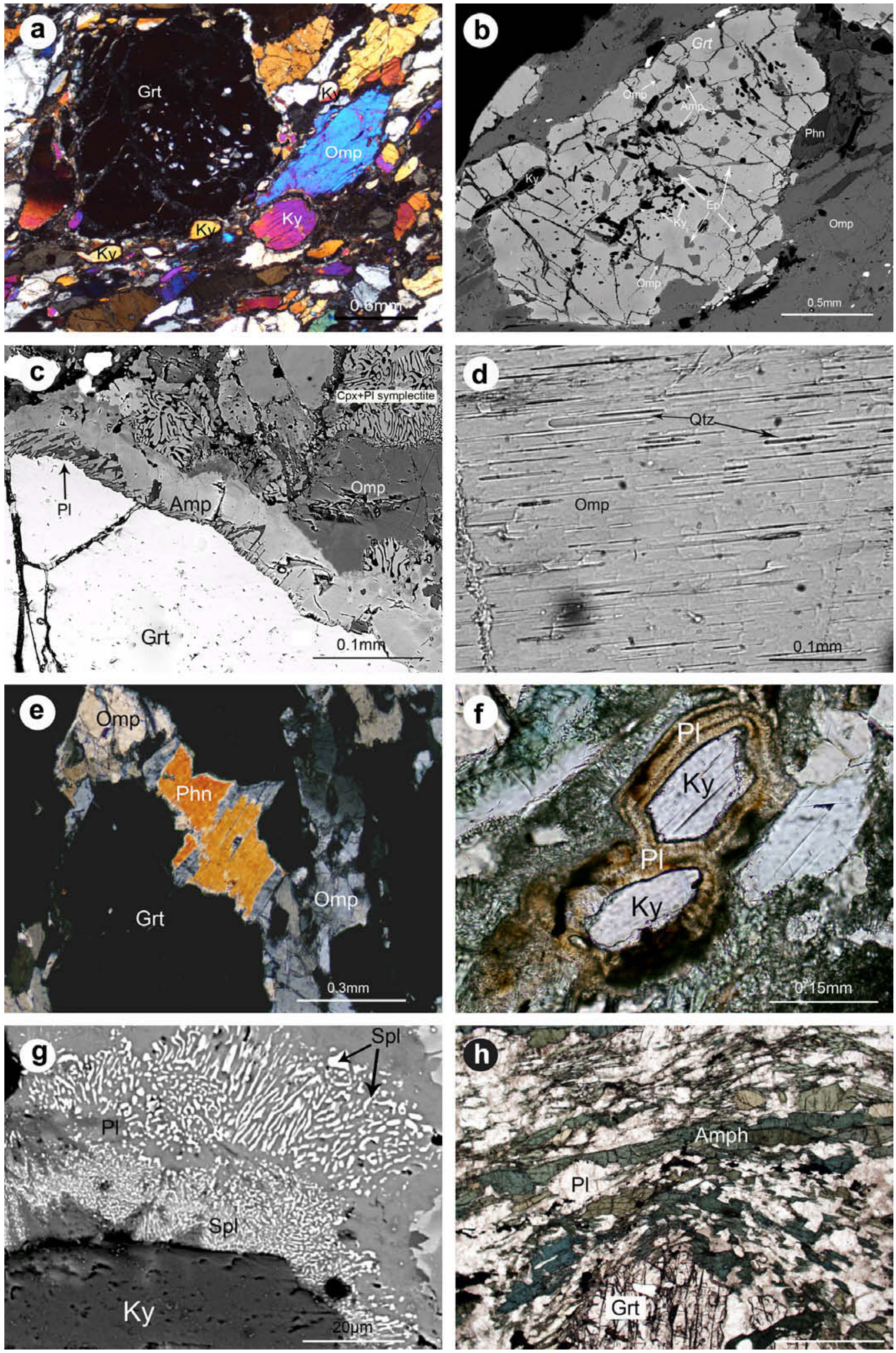

Fig. 3. Photomicrographs illustrating typical textures in eclogite and garnet amphibolite from Shaliuhe terrane, North Qaidam UHPM belt, China. (a) Garnet is surrounded by omphacite and kyanite (5S113, under XPL). (b) Idioblastic garnet containing abundant mineral inclusions (2D06, BSE image). (c) Garnet is surrounded by kelyphite of amphibole and minor plagioclase. Primary omphacite is replaced by vermicular symplectite of Cpx + Pl (2D04, BSE image). (d) Exsolution quartz needles within omphacite (5S113, under XPL). (e) Phengite is partially replaced by biotite (2D07, under XPL). (f) Kyanite porphyroblasts are mantled by fine-grained, dark reaction rims (2D04, under PPL). (g) Kyanite breakdown to Pl + Spl intergrowths (2D04, BSE image). (h) Garnet-amphibolite (5S104, under PPL).

clase (Fig. 3c). Kyanite was replaced by fine-grained symplectite of spinel and plagioclase (Fig. 3f and g). A greenschist-facies assemblage of albite, chlorite, epidote and actinolitic amphibole is readily recognized in some samples.

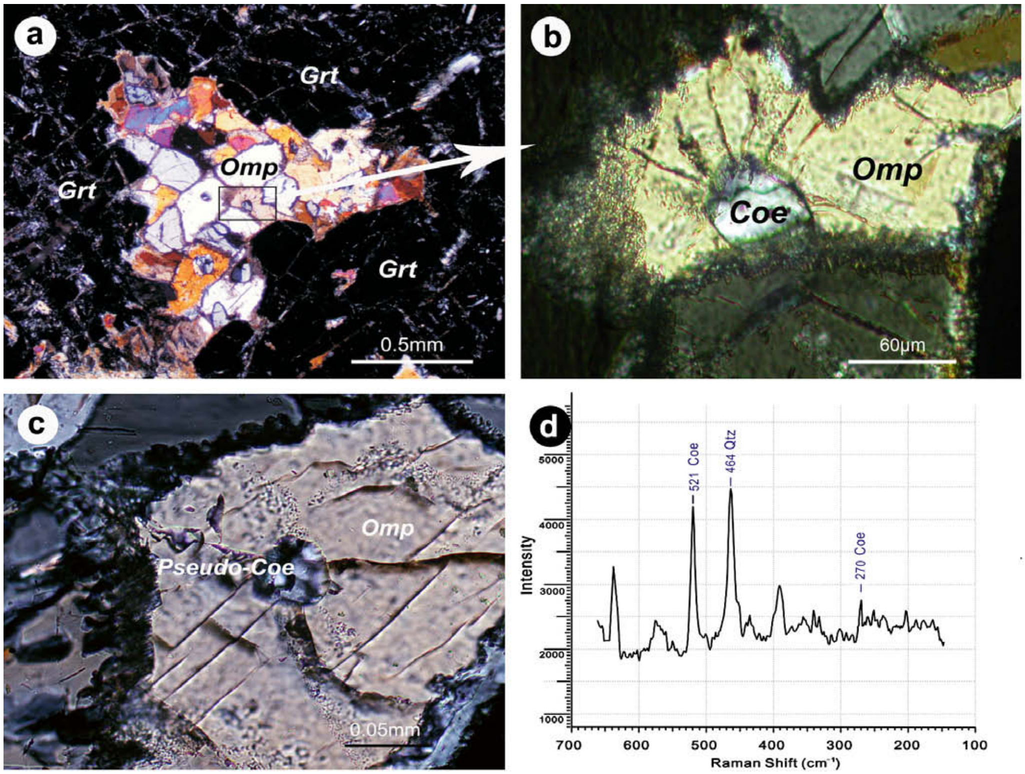

Fig. 4. Microphotographs showing coesite (a and b), quartz pseudomorphs after coesite within omphacite (c), and Raman shift for coesite inclusions (d) from Shaliuhe eclogite.

3.2. Gneiss

The country rock is granitic gneiss (Fig. 2d). It shows a coarse-grained granoblastic texture with strong mylonitization. It consists of K-feldspar, plagioclase, quartz, muscovite, and minor tourmaline.

4. Mineral chemistry

4.1. Analytical method

Chemical compositions of garnet, omphacite, kyanite, phengite, amphibole, epidote and plagioclase from the kyanite-eclogite and garnet-amphibolite were analyzed using a JEOL JXA 8100 electron-microprobe at Peking University. The operating conditions were 15 Kv, 10 nA specimen current, and 40-s counting time per analysis. The ZAF correction was a routine procedure. Both natural and synthetic crystals were used as standards for calibration. Coesite inclusion in thin sections was detected using a Raman micro-spectroscopy (Renishaw RM-1000) with a 514.5 nm line Ar–ion laser at Peking University (see below).

4.2. Results

4.2.1. Coesite inclusion

Among the more than 30 thin sections of eclogite samples studied, coesite pseudomorphs were found in three thin sections; most of them have been retrogressed to fine-grained quartz aggregates

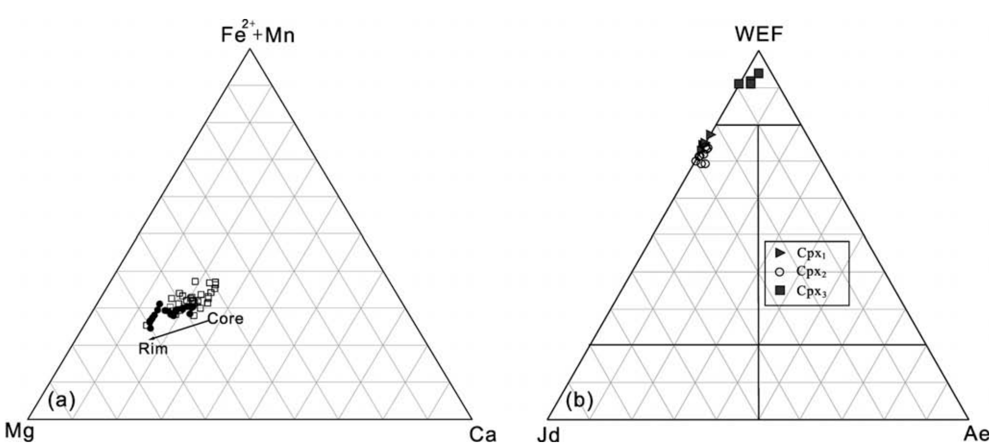

Fig. 5. Ternary diagrams showing compositional variation for garnet (a) and clinopyroxene (b). WEF stands for wollastonite + enstatite + ferrosilite, Jd for jadeite, Ae for aegirine).

(Fig. 4c). In one inclusion, a well-preserved coesite grain was identified within an omphacite crystal, which is in turn preserved in the rim portion of a garnet crystal (Fig. 4c). The omphacite grain is about 0.2–0.3 mm, and the garnet grain is about 12 mm in diameter. In another inclusion, coesite and its retrograde quartz aggregates were surrounded by characteristic radial fracturing in host omphacite (Fig. 4a and b). They together form oval to sub-rounded inclusions of 20–30 μm in size and have pure SiO_2 composition. Similar texture and pseudomorphs of coesite have been previously reported (Chopin, 1984; Smith, 1984). A Raman microspectroscopic analysis shows the characteristic coesite bands at 521 cm^{-1} and 270 cm^{-1} along with the 464 cm^{-1} band for its retrograded quartz (Fig. 4d).

4.2.2. Garnet

End-member compositions of garnet were calculated using Fe^{2+}/Fe^{3+} ratios estimated by charge-balance method with a stoichiometric consideration. Electron probe microanalysis shows that garnet crystals from the eclogite are rich in Mg with X_{Mg} from 0.37 to 0.61, and contain 0.24–0.39 X_{Fe}, 0.14–0.24 X_{Ca} and poor Mn (X_{Mn} < 0.01) (Fig. 5, Table 1). Garnet grains are also zoned as shown in Fig. 6; X_{Mg} increases as X_{Fe} and X_{Ca} decrease from core to rim with X_{Mn} being almost constant. The outmost rims show X_{Mg} decrease, and X_{Fe} and X_{Ca} increase due to retrogression. As garnet X_{Mg} generally increases with increasing metamorphic temperature (Spear, 1989; Mottana et al., 1990), zoning of the eclogitic garnet suggests its growth under a steady temperature increase (Fig. 6).

Table 1
Selected microprobe analyses of garnet in kyanite-eclogite and retrogressed garnet-amphibolite from Shaliuhe terrane, North Qaidam UHPM belt, China.

Sample	2D08	(Ky-Ec)	2D06	(Ky-Ec)	2D05-3	2D07-1.2	2D07-10	2D08-1	2D08-3	4C10-5	5S104					
	Core	Rim	Core	Rim	Kyanite-eclogite						Garnet-amphibolite					
SiO_2	40.93	41.02	40.02	40.61	41.35	40.13	40.93	41.26	42.02	40.15	37.23	38.04	37.37	37.13	37.96	37.36
TiO_2	0.27	0.06	0.10	0.00	0.11	0.07	0.11	0.06	0.08	0.08	0.08	0.05	0.10	0.17	0.01	0.09
Al_2O_3	22.36	22.53	23.24	23.16	22.99	22.54	23.25	23.16	23.44	22.46	21.16	21.23	20.91	21.31	21.67	21.34
Cr_2O_3	0.00	0.01	0.00	0.07	0.04	0.00	0.13	0.00	0.03	0.00	0.00	0.10	0.01	0.05	0.08	0.00
FeO	16.49	15.47	15.72	13.95	15.39	16.09	14.70	15.25	12.44	18.44	24.66	27.72	26.10	25.88	26.96	27.39
MnO	0.91	0.36	0.37	0.21	0.67	0.33	0.29	0.42	0.17	0.87	6.63	3.50	6.00	5.78	1.52	0.37
MgO	10.65	14.51	12.89	16.18	13.19	12.51	13.72	12.44	16.93	10.00	1.91	2.24	1.95	1.70	2.19	2.12
CaO	9.09	6.52	8.20	5.81	6.91	8.21	7.33	7.63	5.51	8.28	7.80	7.76	7.62	7.05	9.43	10.56
Na_2O	0.15	0.00	0.03	0.10	0.05	0.06	0.25	0.03	0.01	0.03	0.06	0.03	0.06	0.02	0.06	0.00
K2O	0.02	0.01	0.00	0.03	0.01	0.01	0.00	0.01	0.01	0.00	0.01	0.01	0.00	0.00	0.00	0.02
Total	100.87	100.51	100.77	100.39	100.71	100.12	100.82	100.26	100.64	100.31	99.59	100.68	100.22	99.09	99.88	99.29
Normalized to eight cations and 12 oxygen																
Si	3.03	3.00	2.94	2.94	3.02	2.97	2.98	3.03	3.01	3.01	2.98	3.01	2.98	2.99	3.01	2.98
Ti	0.02	0.00	0.01	0.00	0.01	0.00	0.01	0.00	0.00	0.01	0.01	0.00	0.01	0.01	0.00	0.01
Al	1.95	1.94	2.01	1.98	1.98	1.97	2.00	2.01	1.98	1.99	2.00	1.98	1.97	2.03	2.02	2.01
Cr	0.00	0.00	0.00	0.00	0.00	0.00	0.01	0.00	0.00	0.00	0.00	0.01	0.00	0.00	0.01	0.00
Fe^{3+}	0.00	0.06	0.11	0.15	0.00	0.09	0.06	0.00	0.00	0.00	0.03	0.00	0.06	0.00	0.00	0.03
Fe^{2+}	1.02	0.89	0.86	0.70	0.94	0.90	0.84	0.94	0.75	1.16	1.62	1.83	1.68	1.74	1.79	1.80
Mn	0.06	0.02	0.02	0.01	0.04	0.02	0.02	0.03	0.01	0.06	0.45	0.24	0.41	0.40	0.10	0.03
Mg	1.18	1.58	1.41	1.75	1.44	1.38	1.49	1.36	1.81	1.12	0.23	0.26	0.23	0.20	0.26	0.25
Ca	0.72	0.51	0.65	0.45	0.54	0.65	0.57	0.60	0.42	0.67	0.67	0.66	0.65	0.61	0.80	0.90
Na	0.02	0.00	0.00	0.01	0.01	0.01	0.04	0.00	0.00	0.00	0.01	0.01	0.01	0.00	0.01	0.00
K	0.00	0.00	0.00	0.00	0.00	0.00	0.00	0.00	0.00	0.00	0.00	0.00	0.00	0.00	0.00	0.00
X_{Fe}	0.34	0.30	0.29	0.24	0.32	0.31	0.29	0.32	0.25	0.39	0.55	0.61	0.57	0.59	0.61	0.60
X_{Mn}	0.02	0.01	0.01	0.00	0.01	0.01	0.01	0.01	0.00	0.02	0.15	0.08	0.14	0.13	0.03	0.01
X_{Mg}	0.40	0.53	0.48	0.60	0.49	0.47	0.51	0.47	0.61	0.37	0.08	0.09	0.08	0.07	0.09	0.08
X_{Ca}	0.24	0.17	0.22	0.15	0.18	0.22	0.20	0.21	0.14	0.22	0.23	0.22	0.22	0.21	0.27	0.30

$X_{Fe} = Fe^{2+}/(Fe^{2+} + Mn + Mg + Ca)$, $X_{Mn} = Mn/(Fe^{2+} + Mn + Mg + Ca)$, $X_{Ca} = Ca/(Fe^{2+} + Mn + Mg + Ca)$ and $X_{Mg} = Mg/(Fe^{2+} + Mn + Mg + Ca)$.

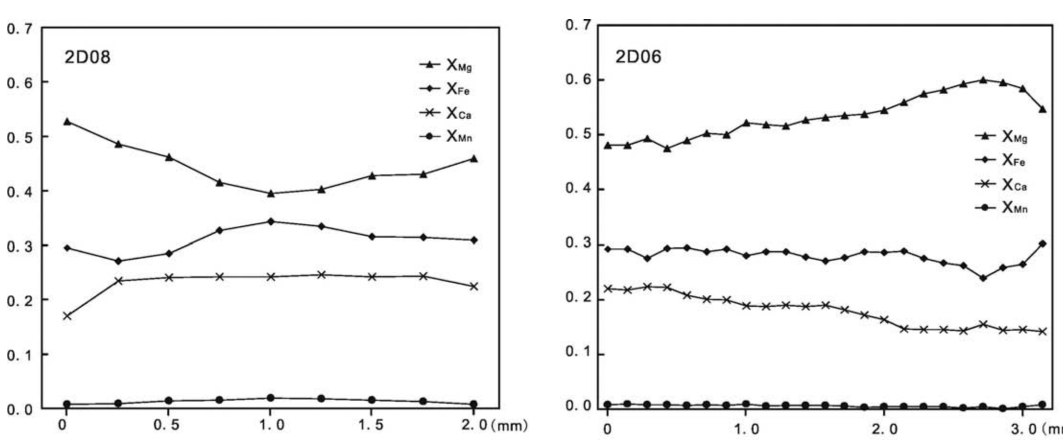

Fig. 6. Representative zoning profiles of $X_{Fe} = Fe^{2+}/(Fe^{2+} + Mn + Mg + Ca)$, $X_{Mn} = Mn/(Fe^{2+} + Mn + Mg + Ca)$, $X_{Ca} = Ca/(Fe^{2+} + Mn + Mg + Ca)$ and $X_{Mg} = Mg/(Fe^{2+} + Mn + Mg + Ca)$ through garnet grains from samples 2D08 and 2D06.

Garnet in the garnet-amphibolite is poor in Mg with X_{Mg} from 0.07 to 0.09, X_{Mn} from 0.01 to 0.16, X_{Ca} from 0.21 to 0.30 and rich in Fe with X_{Fe} from 0.55 to 0.61 (Table 1).

4.2.3. Clinopyroxene

Fe^{3+} content in clinopyroxene was treated as Fe^{3+} = Na–Al–Cr. Clinopyroxene inclusions (Cpx_1) have lesser jadeite (from Jd_{22} to Jd_{28}) content than that of the matrix omphacite (Cpx_2) (Table 2, Fig. 5b). Matrix omphacite (Cpx_2) shows small compositional variation (from Jd_{25} to Jd_{30}). Decompression breakdown of matrix omphacite produces symplectitic aggregates of Na-poor Cpx_3 (Jd < 10%, Fig. 5b) + Pl, some of which were completely replaced by later Amp + Pl.

4.2.4. Phengite

Phengite has homogeneous composition as shown by microprobe analysis and BSE analysis. They have 3.43–3.46 Si per formula based on 11 oxygens (Table 3).

4.2.5. Amphibole

According to the classification scheme of Leake et al. (1997); Fig. 7), amphibole inclusions in garnet cores are edenite/actinolite (Fig. 3b). The corona amphibole around the garnet rims are pargasite. Those associated with the symplectitic Cpx + Pl (after omphacite) are edenite/actinolite (Fig. 3c). The newly formed coarse-grained amphiboles in the garnet-amphibolite (Fig. 3h) are ferropargasite.

4.2.6. Spinel

Only a few spinel grains are large enough for microprobe analysis (Table 4). Fe^{2+} and Fe^{3+} contents were estimated stoichiometrically on the basis of four oxygens and three cations. It is compositionally Mg–Fe–Al spinel with approximately 51–64% hercynite component.

4.2.7. Plagioclase

Plagioclase is present as (1) rare inclusions in garnet cores (Fig. 3b) with composition of An_{83-86} (Table 4); (2) constituents of symplectite after omphacite (Fig. 3c) with composition of An_{20-24} (Table 4); (3) part of kelyphite coronae around garnet associated with amphibole (Fig. 3c), showing pronounced compositional variations (An_{20}–An_{67}) (Table 4); and (4) a newly formed phase in the matrix of the garnet-amphibolite with composition of An_{17}–An_{28} (Table 4, Fig. 3h).

4.2.8. Epidote

The prograde epidote (Ep_1) as inclusions in garnet cores (Fig. 3b) has ~0.18 X_{ps} ($Fe^{3+}/(Fe^{3+}$ + Al)) (Table 4). The retrograde epidote (Ep_2) formed during retrogression stage is generally coarse-grained, and poor in X_{ps}. Some coarse epidote grains are about 3–5 mm, and contain X_{ps} from 0.02 to 0.03 (Table 4).

5. Metamorphic evolution and P-T determination

Preservation of earlier mineral assemblages as inclusions in peak metamorphic minerals and as retrograde overprints altogether enables us to infer the metamorphic histories of the rock samples under investigation. We obtain the P-T path based on thermobarometry and established phase equilibria.

5.1. Pre-peak stage

Pre-peak stage metamorphic conditions can be estimated with confidence using mineral assemblages preserved as inclusions in the peak stage garnet provided that the inclusion minerals had not undergone subsequent re-equilibration among themselves and with the host garnet. Detailed petrography and microprobe analysis indicate that the inclusions have not re-equilibrated with the garnet, and thus retain the original composition. Applications of the Grt-Amp thermometer (Graham and Powell, 1984) and Grt-Amp-Pl-Qtz barometer (Kohn and Spear, 1990) to mineral inclusions and the host garnet yield equilibration temperatures of 410–490 °C and pressures of 0.49–0.67 GPa (see “A” in Fig. 8). This result is consistent with the earlier epidote-amphibolite-facies growth history for garnet.

Table 2
Selected microprobe analyses of clinopyroxene from kyanite-eclogites of Shaliuhe terrane, North Qaidam UHPM belt, China.

Sample	2D06-1.18	2D06-3.23	2D06-1.43	2D05-1	2D05-4	2D07-11	2D07-2	2D07-4	2D08-2	2D08-4	2D08-6	2D08-8	4C10-125.3	4C02-2.7
	Cpx_1			Cpx_2									Cpx_3	
SiO_2	53.77	55.35	54.21	55.45	56.26	55.64	55.59	55.60	55.86	56.08	56.30	55.46	54.03	53.83
TiO_2	0.15	0.15	0.09	0.11	0.04	0.05	0.06	0.10	0.01	0.05	0.00	0.05	0.05	0.33
Al_2O_3	7.51	7.74	6.82	7.14	7.11	7.71	7.45	6.88	7.96	6.66	7.50	7.20	3.76	3.77
Cr_2O_3	0.28	0.04	0.00	0.15	0.03	0.07	0.03	0.00	0.00	0.05	0.00	0.00	0.27	0.41
FeO	2.15	2.28	2.16	1.64	1.72	1.67	1.63	1.89	1.88	1.74	1.57	1.88	3.13	3.48
MnO	0.03	0.09	0.06	0.04	0.00	0.02	0.00	0.00	0.01	0.03	0.05	0.00	0.04	0.10
MgO	12.39	12.53	13.25	13.11	12.70	12.61	12.20	12.71	12.34	13.23	12.43	12.78	14.44	14.35
CaO	19.69	18.57	18.85	18.87	18.54	18.00	18.14	18.55	18.03	19.14	18.55	18.40	22.10	22.82
Na_2O	3.07	3.53	3.93	3.75	3.55	4.37	3.91	3.99	4.39	3.76	3.98	4.37	2.11	1.24
K2O	0.00	0.00	0.01	0.00	0.00	0.00	0.00	0.01	0.00	0.01	0.00	0.00	0.03	0.00
Total	99.04	100.28	99.38	100.26	99.95	100.14	99.01	99.73	100.48	100.75	100.38	100.14	99.96	100.33
Cations per six oxygen atoms														
Si	1.95	1.98	1.94	1.97	2.01	1.97	2.00	1.99	1.98	1.98	2.00	1.97	1.95	1.96
Ti	0.00	0.00	0.00	0.00	0.00	0.00	0.00	0.00	0.00	0.00	0.00	0.00	0.00	0.01
Al	0.32	0.33	0.29	0.30	0.30	0.32	0.32	0.29	0.33	0.28	0.31	0.30	0.16	0.16
Cr	0.01	0.00	0.00	0.00	0.00	0.00	0.00	0.00	0.00	0.00	0.00	0.00	0.01	0.01
Fe^{3+}	0.00	0.00	0.00	0.02	0.02	0.01	0.03	0.04	0.03	0.03	0.03	0.06	0.07	0.00
Fe^{2+}	0.07	0.07	0.06	0.04	0.05	0.02	0.05	0.05	0.04	0.04	0.05	0.06	0.02	0.11
Mn	0.00	0.00	0.00	0.00	0.00	0.00	0.00	0.00	0.00	0.00	0.00	0.00	0.00	0.00
Mg	0.67	0.67	0.71	0.70	0.68	0.67	0.66	0.68	0.65	0.70	0.66	0.68	0.78	0.78
Ca	0.77	0.71	0.72	0.72	0.71	0.68	0.70	0.71	0.68	0.73	0.71	0.70	0.86	0.89
Na	0.22	0.24	0.27	0.26	0.25	0.30	0.27	0.28	0.30	0.26	0.27	0.30	0.15	0.09
K	0.00	0.00	0.00	0.00	0.00	0.00	0.00	0.00	0.00	0.00	0.00	0.00	0.00	0.00
Sum	4.00	4.00	4.00	4.01	4.02	3.98	4.02	4.03	4.01	4.02	4.03	4.05	4.00	4.00
Jadeite	0.22	0.25	0.27	0.25	0.25	0.28	0.28	0.27	0.29	0.25	0.28	0.30	0.09	0.09

Table 3
Selected microprobe analyses of phengite and amphibole from kyanite-eclogites and retrogressed garnet-amphibolite of Shaliuhe terrane, North Qaidam UHPM belt, China.

Sample	2D06-11	2D07-01	2D07-2	2D06-2incl. in grt	2D06-5	2D04-1.1	2D04-1.7	2D04-3.2	4C10-125.2	4C10-125.5	5S104-1.4	5S104-2.1	5S104-4.2
	Kyanite-eclgoite										Garnet-amphibolite		
	Phn			Amp incl. in Grt		Amp corona around Grt			Amp symplectite		Amp		
SiO2	52.84	52.41	52.46	50.72	53.38	40.28	40.65	40.32	56.32	48.53	39.84	40.22	39.75
TiO2	0.40	0.27	0.37	0.05	0.00	0.02	0.06	0.02	0.04	0.41	0.63	0.53	0.17
Al2O3	26.81	26.63	27.37	8.89	5.99	21.13	18.93	18.56	6.08	8.77	14.42	14.87	14.00
Cr2O3	0.30	0.14	0.18	0.00	0.03	0.05	0.06	0.05	0.14	0.15	0.02	0.00	0.00
FeO	0.95	1.07	1.03	3.79	3.96	11.12	10.92	11.84	3.53	6.82	19.43	19.14	21.48
MnO	0.10	0.00	0.01	0.07	0.05	0.12	0.09	0.10	0.11	0.03	0.46	0.46	0.42
MgO	4.37	4.11	4.11	19.60	20.48	11.61	12.41	11.81	14.61	17.80	7.83	7.36	6.82
CaO	0.00	0.00	0.00	10.44	11.27	10.75	11.15	11.30	13.35	12.58	11.00	11.04	10.88
Na2O	0.30	0.42	0.50	1.86	1.30	3.17	3.21	3.17	1.92	1.84	2.16	1.86	2.08
K2O	9.44	10.52	10.49	0.01	0.07	0.13	0.07	0.19	0.09	0.31	0.72	0.66	0.74
Total	95.57	95.58	96.53	95.64	96.75	98.72	97.91	97.68	96.19	97.24	97.38	96.99	97.30
Si	3.46	3.46	3.43	7.14	7.42	5.77	5.88	5.88	7.87	6.91	7.86	7.93	7.91
Ti	0.02	0.01	0.02	0.01	0.00	0.00	0.01	0.00	0.00	0.04	0.09	0.08	0.03
Al	2.07	2.07	2.11	1.48	0.98	3.57	3.23	3.19	1.00	1.47	3.35	3.46	3.29
Cr	0.02	0.01	0.01	0.00	0.00	0.01	0.01	0.01	0.02	0.02	0.00	0.00	0.00
Fe^{3+}	0.03	0.00	0.00	0.22	0.23	0.37	0.41	0.36	0.00	0.13	1.28	1.26	1.43
Fe^{2+}	0.03	0.06	0.06	0.22	0.23	0.96	0.91	1.08	0.41	0.68	1.92	1.89	2.15
Mn	0.01	0.00	0.00	0.01	0.01	0.02	0.01	0.01	0.01	0.00	0.08	0.08	0.07
Mg	0.43	0.40	0.40	4.11	4.24	2.48	2.67	2.57	3.04	3.78	2.30	2.16	2.02
Ca	0.00	0.00	0.00	1.57	1.68	1.65	1.73	1.77	2.00	1.92	2.33	2.33	2.32
Na	0.04	0.05	0.06	0.51	0.35	0.88	0.90	0.90	0.52	0.51	0.83	0.71	0.80
K	0.79	0.89	0.88	0.00	0.01	0.02	0.01	0.04	0.02	0.06	0.18	0.17	0.19
Total	6.88	6.96	6.96	15.26	15.16	15.71	15.76	15.80	14.89	15.52	20.23	20.07	20.20

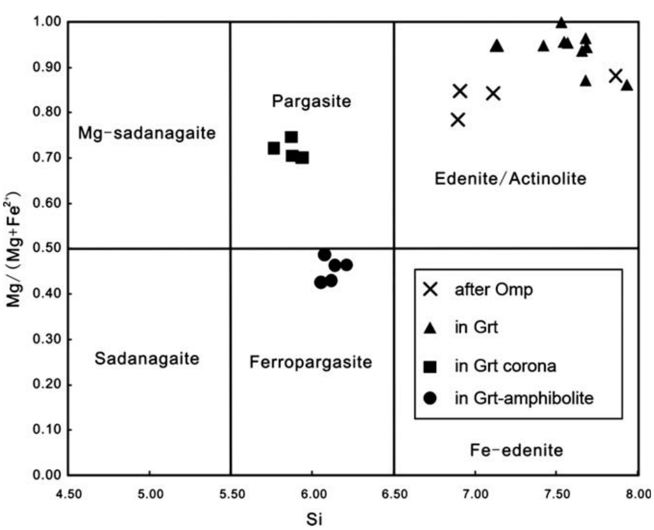

Fig. 7. Classification diagram for amphibole in kyanite-eclogite following Leake et al. (1997). Amphibole in the coronae after garnet is plotted in the pargasite compositionally field, whereas amphibole in the symplectite after omphacite and inclusion preserved in garnet core regions are mainly edenite/actinolite.

5.2. Peak stage

The presence of coesite inclusions demonstrates the UHP metamorphism in the coesite stability field for the peak stage. The peak stage mineral assemblage is Grt + Omp + Ky + Rt + Phn. Using the Grt-Omp-Phn-(Ky) thermobarometry of Ravna and Terry (2004), the intersection of the Grt-Cpx-Phn and Grt-Cpx-Ky-SiO_2 thermobarometric curves in P-T space offers the best P-T estimates for peak conditions of the kyanite-eclogite. Highest $X_{Mg}/(X_{Mg} + X_{Fe})$ ratio at, or close to, garnet grain rims has been used to determine the peak P-T conditions (Carswell et al., 1997) as listed in Table 1. To avoid retrograde effect, we selected three freshest samples, chose highest jadeite content for omphacite (Holland, 1980) and highest Si content (Massonne and Schreyer, 1987) for phengite. We thus obtained the peak conditions of P = 2.7–3.4 GPa, T = 610–700 °C which is located in coesite stable region (see "B" in Fig. 8).

5.3. Retrogression stage

Retrograde metamorphism could take place under a wide range of P-T conditions during exhumation with and/or without obvious temperature changes. Consequently, retrograde reactions can be varied and take different forms. Here we focus on several major textural relationships and some obvious retrograde mineral assemblages (e.g. garnet-amphibolite assemblage): garnet rims are replaced by kelyphitic amphibole and plagioclase; Omphacite breaks down to intergrowths of clinopyroxene and plagioclase, which is replaced again by later amphibole and plagioclase; Kyanite is replaced by fine-grained symplectite of spinel and plagioclase.

Coronae of amphibole and plagioclase around garnet are formed where garnet is in contact with matrix omphacite (Fig. 2c). Using the Grt-Amp thermometer (Graham and Powell, 1984) on Grt-Amp (green)-Pl retrograde rim pairs, we obtained equilibration temperature of 645–725 °C. Using the Grt-Amp-Pl-Qtz barometer of Kohn and Spear (1990), we obtained equilibration pressures of 0.9–1.3 GPa. Using the Cpx-Pl-Qtz barometer (Ellis, 1980) on Cpx-Pl compositions of symplectite as a result omphacite breakdown gives equilibration pressures of 1.2–1.3 GPa (see "C" in Fig. 8).

While these estimates are significant, the decompression reaction assemblages (breakdowns and replacements) used are likely transient features and may actually represent "meta-stable" equilibrium. For example, "eclogitic amphiboles" are generally in disequilibrium with garnet (Graham and Powell, 1984). Hence, we can also estimate retrograde conditions associated with the more stable garnet-amphibolite assemblage. Using the Grt-Amp thermometer (Graham and Powell, 1984) and the Grt-Amp-Pl-Qtz barometer (Kohn and Spear, 1990), the P-T conditions of P = 0.7–1.0 GPa, T = 630–720 °C have been obtained (see "D" in Fig. 8).

Table 4
Selected microprobe analyses of spinel, plagioclase, epidote and margarite from eclogite and garnet-amphibolite of Shaliuhe terrane, North Qaidam UHPM belt, China.

Sample	2D04-7.1	2D05-1	4C02-4.1	4C02-2.1	2D04-6.3	2D04-1.3	4C10-7	2D04-13	4C-10-4	5S07-125.2	5s104-1.6	5s104-2.2	4C01-1	4C01–2
	Kyanite-eclogite										Garnet-amphibolite			
	spl		pl icl. in grt		pl corona around grt		pl symplectite after Cpx^2		Ep^1	Ep^2	pl		Mrg	
SiO_2	0.19	0.17	68.16	45.08	64.61	51.68	62.90	66.19	38.66	39.25	63.96	60.88	30.59	30.01
TiO_2	0.07	0.03	0.00	0.05	0.03	0.00	0.01	0.05	0.16	0.08	0.04	0.00	0.03	0.00
Al_2O_3	61.52	63.30	20.07	34.19	23.16	29.98	22.91	20.49	25.81	32.08	22.71	24.41	50.85	50.51
Cr_2O_3	0.32	1.14	0.06	0.00	0.00	0.00	0.00	0.00	0.00	0.01			0.00	0.00
FeO	28.45	23.01	0.45	0.66	0.38	0.38	0.08	0.22	7.98	1.34	0.46	0.26	0.49	0.30
MnO	0.52	0.40	0.00	0.00	0.08	0.03	0.00	0.00	0.04	0.00	0.17	0.03	0.00	0.00
MgO	8.52	11.45	0.03	0.10	0.02	0.03	0.06	0.30	0.05	0.04	0.00	0.00	0.59	0.23
CaO	0.29	0.06	1.04	17.68	4.15	13.60	4.55	2.58	23.41	24.62	3.64	5.82	11.35	12.74
Na_2O	0.05	0.07	10.89	1.65	9.01	3.75	9.90	10.11	0.00	0.06	6.89	9.34	1.65	0.88
K2O	0.01	0.00	0.05	0.00	0.01	0.02	0.04	0.03	0.01	0.01	2.72	0.08	0.01	0.06
Total	99.94	99.63	100.75	99.41	101.45	99.47	100.45	99.97	96.12	97.49	100.64	100.85	95.57	94.73
Si	0.005	0.005	2.96	2.09	2.81	2.36	2.78	2.91	3.051	3.00	2.82	2.70	2.02	2.01
Ti	0.001	0.001	0.00	0.00	0.00	0.00	0.00	0.00	0.009	0.01	0.00	0.00	0.00	0.00
Al	1.974	1.985	1.03	1.87	1.19	1.61	1.19	1.06	2.401	2.89	1.18	1.28	3.96	3.98
Cr	0.000	0.000	0.00	0.00	0.00	0.00	0.00	0.00	0.000	0.00			0.00	0.00
Fe^{3+}	0.007	0.023	0.02	0.00	0.00	0.00	0.00	0.00	0.527	0.09	0.00	0.00	0.02	0.00
Fe^{2+}	0.648	0.512	0.00	0.03	0.01	0.02	0.00	0.01	0.000	0.00	0.02	0.01	0.01	0.02
Mn	0.012	0.009	0.00	0.00	0.00	0.00	0.00	0.00	0.003	0.00	0.00	0.00	0.00	0.00
Mg	0.346	0.454	0.00	0.00	0.00	0.00	0.00	0.00	0.006	0.01	0.01	0.00	0.06	0.02
Ca	0.008	0.002	0.05	0.88	0.19	0.67	0.22	0.12	1.979	2.02	0.17	0.28	0.80	0.91
Na	0.003	0.004	0.92	0.15	0.76	0.33	0.85	0.86	0.000	0.01	0.59	0.80	0.21	0.11
K	0.000	0.000	0.00	0.00	0.00	0.00	0.00	0.00	0.001	0.00	0.15	0.01	0.00	0.01
Sum	3.004	2.993	4.98	5.02	4.97	4.99	5.04	4.97	7.977	8.01	4.95	5.07	7.09	7.06

Ep^1(incl. in grt.), Ep^2 (etrogression).

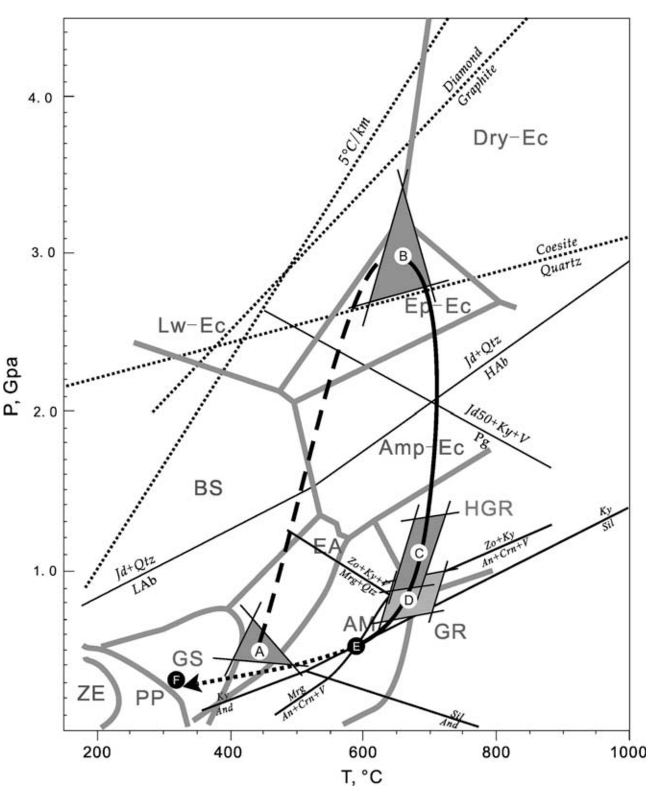

Fig. 8. P-T path for kyanite-eclogite from Shaliuhe terrane, North Qaidam UHPM belt, China (after Liou et al., 1998). A, pre-peak stage; B, peak stage; C, retrograde stage, calculated based on reaction textures of Grt and Omp; D, retrogrde stage, calculated using Grt-Amp-Pl in garnet-amphibolite; E, retrograde stage, based on the reaction anorthite + corundum + H_2O = margarite (Gibson, 1979); F, retrograde stage, based on the latest mineral assemblage: Ab + Chl + Ep + Act.

During retrogression, kyanite in the kyanite-eclogite is often replaced by the symplectitic Pl + Spl assemblage (plus corundum or sapphirine if there is a temperature increase) (Godard and Mabit, 1998). Godard and Mabit (1998) also pointed out that both kyanite and omphacite breakdowns are coupled during retrogression, and the required silica for quartz-free eclogite can be gained from kyanite destabilization. Meanwhile, we think that the required Ca, Fe, Mg and Na to form spinel and plagioclase must come from the matrix minerals (e.g. garnet and omphacitic Cpx) through diffusion. So the P-T conditions of kyanite breakdown may be consistent with symplectite formation after omphacite, and may also be contemporaneous with the formation of kelyphitic garnet rims (i.e. “C” in Fig. 8). The formation of later margarite in the former kyanite domains from the garnet amphibolite indicate that the reaction anorthite + corundum + H_2O = margarite (Gibson, 1979) may have occurred. This reaction implies that the retrogression path has crossed this curve at P-T conditions below 650 °C and 0.5 GPa (See “E” in Fig. 8).

A greenschist-facies assemblage of Act + Chl + Ab + Qtz was overprinted during the final uplift (see “F” in Fig. 8).

6. Zircon SHRIMP dating of kyanite-eclogite

6.1. Analytical techniques

Eclogite samples were crushed and sieved to <300 μm. Zircon grains were separated by magnetic and heavy liquid techniques, and finally hand-picked under a binocular. The separated zircon grains were embedded in 25 mm epoxy discs and then polished down to about half thickness. The zircon standard Temora (417 Ma) (Black et al., 2003) was also cast in the mount for analysis. Mineral inclusions in zircons were detected using laser Raman microspectroscopy at Peking University. Cathodoluminescence (CL) imaging of sample was carried out at Peking University using a FEI PHILIPS XL30 SFEG SEM with 2-min scanning time at conditions of 15 kV and 120 μA. U, Th and Pb were analyzed by SHRIMPII at Beijing SHRIMP center, Chinese Academy of Geosciences. Instrumental conditions and measurement procedures were similar to those reported previously (Compston et al., 1992; Stern, 1998; Williams, 1998). CL images and photomicrographs were used to inspect zircon grains and select analytical spots. Spot size of 25–

30 μm and a primary O_2^- ion beam of 9 μA were applied during the analysis. The age determination for each spot was collected in sets of five scans through mass peaks. The Temora zircon standard was analyzed first, and repeated after every 3–4 analyses of samples. The squid (Ludwig, 2002) and isoplot programs (Ludwig, 1997) were used for data processing and measured ^{204}Pb was applied for the common lead correction. Results are given in Table 5 with 2σ errors.

6.2. Zircon internal structure, inclusions and SHRIMP data

One fresh kyanite-eclogite sample (4C05) was studied for zircon U–Th–Pb SHRIMP geochronology. Zircon crystals recovered from this sample are colorless, rounded or ovoid with 140–200 μm across (Fig. 9). Rare garnet, omphacite and rutile inclusions are identified by Raman microspectroscopy. No coesite inclusions were found. Although CL images of some zircon grains show inherited magmatic "morphology", weak fir-tree zoning features characteristic of zircons in granulite-facies rocks (Vavra et al., 1996) and eclogite or gabbro (Rubatto et al., 1999; Rubatto and Gebauer, 2000) are obvious (Fig. 9a and c). Magmatic core is well preserved in some grains (Fig. 9b). Most zircon grains are surrounded by stronger luminescence rims. The uranium content in zircons varies significantly from 70 to 442 ppm, and Th/U ratios from 0.36 to 0.76 (except for three higher ratios 0.93–1.19) (Table 5). Ten analyses of zircon yielded ^{204}Pb corrected $^{206}Pb/^{238}U$ ages ranging from 419 ± 12 Ma to 478 ± 16 Ma. These analyses plot on concordia (Fig. 10), and define a concordia age of 440 ± 6 Ma (n = 10).

Table 5
U, Th and Pb SHRIMP zircon data of kyanite-eclogite from Shaliuhe terrane, North Qaidam UHPM belt, China.

Sample	^{206}Pbc[%]	U[ppm]	Th[ppm]	Th/U	$^{206}Pb^*$ [ppm]	$^{207}Pb^*/^{206}Pb^*$	±%	$^{207}Pb^*/^{235}U$	±%	$^{206}Pb^*/^{238}U$	±%	$^{206}Pb/^{238}U$ Age	
4C05-1.1	3.47	263	151	0.59	16.6	0.0541	12	0.530	12	0.0711	2.3	443	±10.0
4C05-3.1	1.69	336	201	0.62	21.6	0.0587	8.6	0.595	8.9	0.0654	2.2	457	± 9.7
4C05-4.1	1.73	434	439	1.05	27.5	0.0590	6.9	0.589	7.3	0.0735	2.2	451	± 9.4
4C05-5.1	2.17	472	424	0.93	28.8	0.0571	7.0	0.547	7.3	0.0724	2.1	433	± 8.9
4C05-6.1	1.42	590	680	1.19	37.1	0.0566	4.7	0.564	5.1	0.0695	2.1	450	± 9.1
4C05-8.1	2.50	246	134	0.56	14.7	0.0603	13	0.563	13	0.0722	2.4	423	± 9.8
4C05-9.1	7.61	109	43	0.41	6.79	0.041	38	0.38	38	0.08	3.0	419	±12.0
4C05-10.1	1.06	408	259	0.66	25.2	0.0603	5.3	0.591	5.7	0.0678	2.1	443	± 9.1
4C05-12.1	3.08	344	182	0.55	21.7	0.0491	14	0.482	14	0.0672	2.2	443	± 9.4
4C05-2.2	5.80	70	24	0.36	4.90	0.060	32	0.63	32	0.0711	3.4	478	±16.0
4C05-13.1	3.52	246	182	0.76	15.1	0.0480	17	0.456	17	0.0615	2.4	429	± 9.9

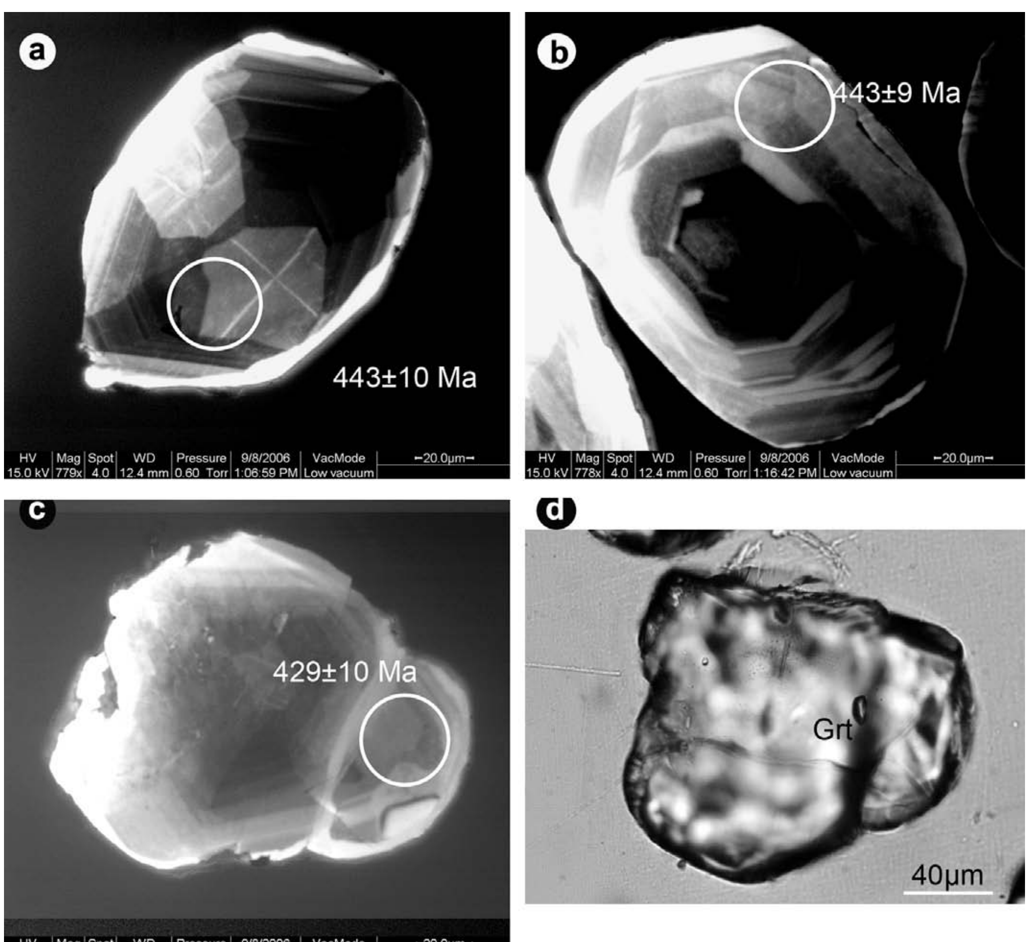

Fig. 9. Cathodoluminescence (CL) images (a–c) showing internal structures (weak fir-tree zoning and strong light rims) of zircons from the eclogite (sample 4C05) and zircon photomicrographs (d) showing inclusions of garnet (Grt) (under PPL).

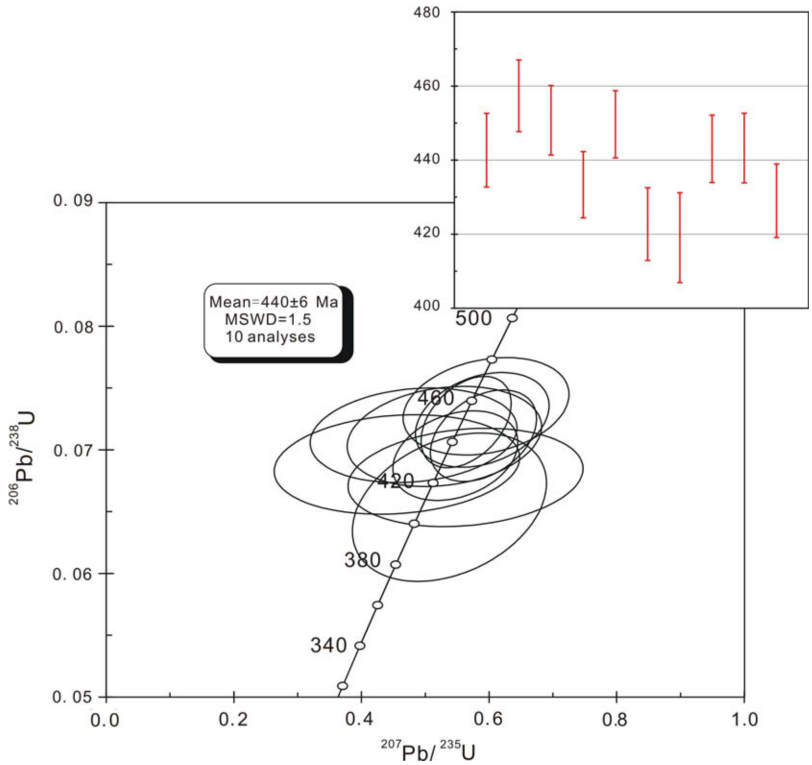

Fig. 10. Concordia diagram showing results of zircon SHRIMP analyses from the kyanite-eclogite (sample 4C05). Error ellipses are 2σ.

7. Discussion and conclusions

While the nature of UHP metamorphism in the North Qaidam has been recognized for several years, direct and convincing evidence for UHP metamorphism of eclogite is lacking. Indirect lines of evidence include coesite inclusions from paragneiss zircons in the Dulan terrane (Yang et al., 2001; Song et al., 2003a), diamond inclusion preserved in a zircon crystal, exsolution textures preserved in garnet and olivine from the Luliangshan garnet peridotite (Song et al., 2004; Song et al., 2005), and coesite pseudomorphs and quartz exsolutions in eclogite (Song et al., 2003a; Zhang et al., 2005b; Yang et al., 2005). These observations, however, remain controversial (Hermann et al., 2005; Page et al., 2005; Smith, 2005). The coesite inclusions reported here represent unequivocal evidence for UHP metamorphism for the North Qaidam eclogite and deep subduction of oceanic lithosphere (Zhang et al., 2008) and continental crustal materials (Song et al., 2005b; Zhang et al., 2008). Recently, well-preserved coesite inclusion has also been recognized in Aercitoushan, North Qaidam (Zhang et al., 2009), which further suggests some eclogites in Dulan have undergone UHP metamorphism definitely.

The metamorphic evolution of the Shaliuhe kyanite-eclogite, in terms of a P-T path, is given in Fig. 8. Information on the pre-peak stage metamorphism is represented by the mineral inclusions in zoned garnets. The inclusion assemblage Amp + Ep + Pl + Qtz in garnet interiors indicate that garnets began to grow in the epidote-amphibole-facies before entering the eclogite-facies (Fig. 8). Grt-Amp-Pl thermobarometry calculations using inclusion mineral assemblages yield $P = 0.4$–0.7 GPa and $T = 410$–490 °C, which is consistent with the growth in the epidote-amphibolite facies. The prograde path may be associated with pressure increase during lithosphere subduction before reaching the peak metamorphic stage. The peak stage P-T conditions are constrained by the Grt-Omp-Phn-Ky thermobarometry at $P = 2.7$–3.4 GPa and $T = 610$–700 °C. The maximum pressure of peak metamorphic stage is consistent with the presence of coesite inclusions in omphacite.

The garnet reaction rims, the breakdown of omphacite, symplectite of kyanite and the garnet-amphibolite record the retrogression. The P-T estimations define a very steep "subduction" path (dashed line) before reaching the peak eclogite-facies (Fig. 8). The exhumation is characterized by an almost isothermal decompression path. Then, the rocks cooled through amphibolite facies. The intersection of the retrogression path with the Ky-Sil univariant curve marks the formation of late margarite surrounding kyanite. Although we did not obtain precise P-T conditions for the latest retrogression, the overprint mineral assemblage records the greenschist-facies conditions. Although the shape, CL patterns and the higher Th/U ratios (e.g. 0.93–1.19) of zircons from the kyanite-eclogite retain magmatic features, a significant metamorphic resetting can be recognized. The rare garnet and rutile inclusions in some zircon grains (Fig. 9d) also indicate that the 440 Ma may represent the time of the HP/UHP metamorphism. Some grains are surrounded by narrow, stronger luminescence rims, which may record the later overprint during exhumation. This age is similar to ages obtained using whole-rock Sm–Nd isochron method and SHRIMP Zircon U–Pb technique on samples from the Dulan terrane (Song et al., 2003a, 2006; Mattinson et al., 2006). Mattinson et al. (2006) suggested a long duration for UHP metamorphism (422–449 Ma); our 440 Ma HP/UHP metamorphic age in this study is within this age range. However, the younger age limit by these authors may in fact represent the retrograde overprint as mentioned before (Table 5).

As the eclogite was formed from an ocean crust protolith (Zhang et al., 2008), the prograde path would represent the P-T path of a subducting slab (see above and also Fig. 8). The preservation of epidote-amphibolite-facies mineral inclusions in garnet and the garnet zoning point to rapid oceanic crust subduction followed by subduction of continental crustal materials (Song et al., 2003b, 2005b) before exhumation in response to the continental collision

(Song et al., 2005b, 2006). The calculated geothermal gradient during subduction is less than 18–24 °C $kbar^{-1}$ (or ~6–8 °C km^{-1}). This gradient suggests a relatively "cold" subduction path. Cold thermal gradients in subduction zones may be due to many reasons, e.g., old age of subducting crust, refrigeration from a continuously down-going slab, or fast subduction rate (Cloos, 1985; Peacock, 1987). The protolith age of this kyanite-eclogite is ~514 Ma (Zhang et al., 2008), whereas the metamorphic age is ~440 Ma. The ~80 m.y. old oceanic crust may not be cold enough. Thus the latter two factors might be important. During subduction, fast down-going and refrigeration of continued subduction of oceanic crust can produce a cold prograde metamorphic path. For retrograde processes, eclogite from subduction zones without being followed by continental collision are often characterized by retrograde paths similar to the prograde process paths. In contrast, high pressure metamorphic rocks from continental collision zones show higher temperature retrogression signatures due to the lack of a refrigeration effect (Ernst, 1988). So, high pressure granulite-facies overprints on eclogites are usually observed (O'Brien and Rötzler, 2003) during exhumation. The kyanite-eclogite in this study suggests a slight temperature increase during exhumation probably related to continental material subduction and continental collision (Song et al., 2006).

Current metamorphic evolution models for the North Qaidam eclogite vary in different study area. Only the prograde path of Yuka eclogites has been quantitatively constrained (Chen et al., 2005; Zhang et al., 2005b), which suggests rapid subduction and near isothermal decompression. The eclogite from the north Dulan sub-belt experienced similar decompression path. In contrast, eclogites from Xitieshan and south Dulan sub-belt recorded granulite-facies overprint during their exhumation (Song et al., 2003a; Zhang et al., 2005b), which suggested a slower exhumation process. The kyanite-eclogite P-T path in this study suggests a low geothermal gradient and rapid prograde subduction. The near isothermal (slight temperature increase; see Fig. 8) decompression indicates a rapid exhumation. In brief, the oceanic crust has subducted to depth in excess of >75 km (i.e. above coesite stable region) with relatively rapid exhumation in response to continental collision during the later Ordovician.

Acknowledgements

We are most grateful to G.M. Shu, Z.Q. Yang for their help with the laboratory work. Profs. J.G. Liou, X. Liu, R.Y., Zhang and I. Katayama are also appreciated for their constructive review, which helps make a better presentation of this version. This study was supported by the National Natural Science Foundation of China (Grants 40821002 and 40802016) and Major State Basic Research Development Program (Grants 2009CB825007).

References

Black, L.P., Kamo, S.L., Allen, C.M., Aleinikoff, J.K., Davis, D.W., Korsch, R.J., Foudoulis, C., 2003. TEMORA 1: a new zircon standard for Phanerozoic U–Pb geochronology. Chemical Geology 200, 155–170.

Bucher, K., Fazis, Y., Capitani, C., Grapes, R., 2005. Blueschists, eclogites, and decompression assemblages of the Zermatt-Saas ophiolite: High-pressure metamorphism of subducted Tethys lithosphere. American Mineralogist 90, 821–835.

Carswell, D.A., O'Brien, P.J., Wilson, R.N., Zhai, M.G., 1997. Thermobarometry of phengite-bearing eclogites in the Dabie Mountains of Central China. Journal of Metamorphic Geology 15, 239–252.

Chen, D.L., Sun, Y., Liu, L., Zhang, A.D., Luo, J.H., Wang, Y., 2005. Metamorphic evolution of the Yuka eclogite in the North Qaidam, NW China: evidence from the compositional zonation of garnet and reaction texture in the rock. Acta Petrologica Sinica 21 (4), 1039–1048.

Chen, D.L., Sun, Y., Liu, L., 2007. In Situ LA-ICP-MS zircon U-Pb age of ultrahigh-pressure eclogites in the Yukahe area, northern margin of the Qaidam basin. Science in China (Series D) 37, 279–287. in Chinese.

Chopin, C., 1984. Coesite and pure pyrope in high-grade blueschists of the western Alps: a first record and some consequences. Contributions to Mineralogy and Petrology 86, 107–118.

Cloos, M., 1985. Thermal evolution of convergent plate margins: thermal modeling and reevaluation of isotopic Ar-ages for blueschists in the Franciscan Complex, California. Tectonics 4, 421–433.

Compston, W., Williams, I.S., Kirschvink, J.L., Zhang, Z., 1992. Zircon U–Pb ages for the Early Cambrian time-scale. Journal of the Geological Society of London 149, 171–184.

Ellis, D.J., 1980. Osumilite-sapphirine-quartz granulites from Enderby Land, Antartica: P-T conditions of metamorphism, implications for garnet-cordierite equilibria and the evolution of the deep crust. Contributions to Mineralogy and Petrology 74, 201–210.

Ernst, W.G., 1988. Tectonic history of subduction zones inferred from retrograde blueschist P–T paths. Geology 16, 1081–1084.

Gibson, G.M., 1979. Margarite in Kyanite- and Corundum-Bearing Anorthosite, Amphibolite, and Hornblendite From Central Fiordland, New Zealand. Contributions to Mineralogy and Petrology 68, 171–179.

Godard, G., Mabit, J.L., 1998. Peraluminous sapphirine formed during retrogression of a kyanite-bearing eclogite from Pays de Léon, Armorican Massif, France. Lithos 43, 15–29.

Graham, C.M., Powell, R., 1984. A garnet-hornblende geothermometer: calibration, testing and application to the Pelona Schist, Southern California. Journal of Metamorphic Geology 2, 13–31.

Hermann, J., O'Neill, H.S.C., Berry, A.J., 2005. Titanium soubility in olivine in the system TiO2-MgO-SiO2: no evidence for an ultra-deep orgin of Ti-bearing olivine. Contributions to Mineralogy and Petrology 148, 746–760.

Holland, T.J.B., 1980. The reaction albite = jadeite + quartz determined experimentally in the range 600-1200 °C. American Mineralogist 65, 125–134.

Jahn, B.M., 1999. Sm–Nd isotope tracer study of UHP metamorphic rocks: implications for continental subduction and collisional tectonics. International Geology Review 41, 859–885.

Jahn, B.M., Fan, Q.C., Yang, J.J., Henin, O., 2003. Petrogenesis of the Maowu pyroxenite-eclogite body from the UHP metamorphic terrane of Dabieshan: chemical and isotopic constraints. Lithos 70, 243–267.

Kohn, M.J., Spear, F.S., 1990. Two new geobarometers for garnet amphibolites, with applications to southeastern Vermont. American Mineralogist 75, 89–96.

Kretz, R., 1983. Symbols for rock-forming minerals. American Mineralogist 68, 277–279.

Leake, B.E., Woolley, A.R., Arpes, C.E.S., et al., 1997. Nomenclature of amphiboles: report of the Subcommittee on amphiboles of the International Mineralogical Association, Commission on New Minerals and Mineral Names. American Mineralogist 82, 1019–1037.

Liou, J.G., Zhang, R.Y., 2002, third ed. Ultrahigh-pressure metamorphic rocks: Encyclopedia of Physical sciences and technology, vol. 17 Academia Press, Tarzana, CA. pp. 227–244.

Liou, J.G., Zhang, R.Y., Ernst, W.G., Rumble, D., Maruyama, S., 1998. High-pressure minerals from deeply subducted metamorphic rocks. Review of Mineralogy 37, 33–96.

Liou, J.G., Tsujimori, T., Zhang, R.Y., Katayama, I., Maruyama, S., 2004. Global UHP metamorphism and continental subduction/collision: The Himalayan model. International Geology Review 46, 1–27.

Liu, L., Che, Z.C., Wang, Y., Luo, J.H., Chen, D.L., 1999. The petrological characters and geotectonic setting of high-pressure metamorphic rock belts in Altun Mountains. Acta Petrologica Sinica 15 (01), 57–64. in Chinese with English abstract.

Ludwig, K.R., 1997. Using Isoplot/EX, version 2. In: A Geochronological Toolkit for Microsoft Excel. Berkeley Geochronological Center Special Publication, Berkeley, p. 47.

Ludwig, K.R., 2002. SQUID 1.02, A User's Manual. Berkeley Geochronology Center Special Publication 2, 2455 Ridge Road, Berkeley, CA 94709, USA, p. 22.

Massonne, H.J., Schreyer, W., 1987. Phengite geobarometry base on the limiting assemblage with K-feldspar, phlogopite, and Quartz. Contributions to Mineralogy and Petrology 96, 214–219.

Mattinson, C.G., Wooden, J.L., Liou, J.G., Bird, D.K., Wu, C.L., 2006. Age and duration of eclogite-facies metamorphism, North Qaidam HP/UHP terrane, Western China. American Journal of Science 306, 683–711.

Mattinson, C.G., Menold, C.A., Zhang, J.X., Bird, D.K., 2007. High- and Ultrahigh-Pressure Metamorphism in the North Qaidam and South Altyn Terranes, Western China. International Geology Review 49, 969–995.

Menold, C.A., Manning, C.E., Yin, A., Alex, R.C., Chen, X., 2002. Tectonic evolution of the North Qaidam UHP Complex, Western China. AGU Fall Meeting. Abstract# T51B-1159.

Mottana, A., Carswell, D.A., Chopin, C., Oberhänsli, R., 1990. Eclogite facies mineral parageneses. In: Carswell, D.A. (Ed.), Eclogite Facies Rocks. Blackie, Glasgow, pp. 14–52.

O'Brien, P.J., Rötzler, J., 2003. High-pressure granulites: formation, recovery of peak conditions and implications for tectonics. Journal of Metamorphic Geology 21, 3–20.

Page, F.Z., Essene, E.J., Mukasa, S.B., 2005. Quartz exsolution in clinopyroxene is not proof of ultrahigh pressures: evidence in the ecloigites from the Eastern Blue Ridge, Southern Appalachians, USA. American Mineralogist 90, 1092–1099.

Peacock, S.M., 1987. Creation and preservation of subduction-related inverted metamorphic gradients. Journal of Geophysical Research, B, Solid Earth and Planets 92, 763–781.

Ravna, E.J.K., Terry, M.P., 2004. Geothermobarometry of UHP and HP eclogites and schists - an evaluation of equilibria among garnet-clinopyroxene- kyanite-phengite- coesite/quartz. Journal of Metamorphic Geology 22, 579–592.

Reinecke, T., 1991. Very-high-pressure metamorphism and uplift of coesite-bearing metasediments from the Zermatt-Saas zone, Western Alps. European Journal of Mineralogy 3, 7–17.

Rubatto, D., Gebauer, D., 2000. Use of cathodoluminescence for U–Pb zircon dating by ion microprobe: some examples from the Western Alps. In: Pagel, M., Barbi, V., Blanc, P., Ohnenstetter, D. (Eds.), Cathodoluminescence in geosciences. Springer, Berlin, Heidelberg, New York, pp. 373–400.

Rubatto, D., Gebauer, D., Compagnoni, R., 1999. Dating of eclogite-facies zircons: the age of Alpine metamorphism in the Sesia–Lanzo Zone (Western Alps). Earth and Planetary Science Letters 167, 141–158.

Smith, D.C., 1984. Coesite in clinopyroxene in the Caledonides and its implications for geodynamics. Nature 310, 641–644.

Smith, D.C., 2005. The SHAND quaternary system for evaluating the supersilicic or subsilicic crystal-chemistry of eclogite minerals, and potential new UHPM pyroxene and garnet end-members. Mineralogy and Petrology 88, 87–122.

Song, S.G., 2001. Petrology, Mineralogy and Metamorphic Evolution of the Dulan UHP Terrane in North Qaidam, NW China and its Tectonic Implications. Doctoral Thesis in Institute of Geology, Chinese Academy of Geological Sciences.

Song, S.G., Yang, J.S., Xu, Z.Q., Liou, J.G., Shi, R.D., 2003a. Metamorphic evolution of the coesite-bearing ultrahigh-pressure terrane in the North Qaidam, northern Tibet, NW China. Journal of Metamorphic Geology 21, 631–644.

Song, S.G., Yang, J.S., Liou, J.G., Wu, C.L., Shi, R.D., Xu, Z.Q., 2003b. Petrology, geochemistry and isotopic ages of eclogites from the Dulan UHPM terrane, the North Qaidam, NW China. Lithos 70, 195–211.

Song, S.G., Zhang, L.F., Niu, Y.L., 2004. Ultra-deep origin of garnet peridotite from the North Qaidam ultrahigh-pressure belt, Northern Tibetan Plateau, NW China. American Mineralogist 89, 1330–1336.

Song, S.G., Zhang, L.F., Chen, J., Liou, J.G., Niu, Y., 2005a. Sodic amphibole exsolutions in garnet from garnet-peridotite, North Qaidam UHPM belt, NW China: implications for ultradeep-origin and hydroxyl defects in mantle garnets. American Mineralogist 90, 814–820.

Song, S.G., Zhang, L.F., Su, L., Niu, Y.L., Song, B., 2005b. Geochronology of diamond-bearing zircons in garnet peridotite in the North Qaidam UHPM belt, North Tibetan Plateau: A record of complex histories associated with continental collision. Earth and Planetary Science Letters 234, 99–118.

Song, S.G., Zhang, L.F., Niu, Y.L., Su, L., Song, B., Liu, D.Y., 2006. Evolution from oceanic subduction to continental collision: A case study of the Northern Tibetan Plateau inferred from geochemical and geochronological data. Journal of Petrology 47 (3), 435–455.

Spear, F.S., 1989. Petrologic determination of metamorphic pressure-temperature-time paths. In: Spear, F.S., Peacock, S.M. (Eds.), Metamorphic Pressure-Temperature-Time Paths, Short Course in Geology. American Geophysical Union, Washington DC, pp. 1–55.

Stern, R.A., 1998. High-resolution SIMS determination of radiogenic tracer-isotope ratios in minerals. In: Cabri, L.J., Vaughan, D.J. (Eds.), Modern Approaches to Ore and Environmental Mineralogy. Mineralogical Association of Canada, Short Course Series, vol. 27, pp. 241–268.

Vavra, G., Gebauer, D., Schmid, R., Compston, W., 1996. Multiple zircon growth and recrystallization during polyphase Late Carboniferous to Triassic metamorphism in granulites of the Ivrea Zone (Southern Alps): an ion microprobe (SHRIMP) study. Contributions to Mineralogy and Petrology 122, 337–358.

Williams, I.S., 1998. U–Th–Pb geochronology by ion microprobe. In: McKibben, M.A., Shanks, W.C. (Eds.), Applications of Microanalytical Techniques to Understanding Mineralizing Processes. Reviews in Economic Geology, pp. 1–35.

Yang, J.J., Deng, J.F., 1994. Garnet peridotites and eclogites in the northern Qaidam Mountains, Tibetan plateau: a first record. First Workshop on UHP Metamorphism and Tectonics, ILP Task Group III-6, Stanford, A-20.

Yang, J.S., Xu, Z.Q., Song, S.G., Zhang, J.X., Wu, C.L., Shi, R.D., Li, H.B., Maurice, B., 2001. Discovery of coesite in the North Qaidam Early Palaeozoic ultrahigh pressure metamorphic belt, NW China. Sciences De La Terre Et Des Planetes 333, 719–724.

Yang, J.S., Zhang, J.X., Meng, F.C., Shi, R.D., Wu, C.L., Xu, Z.Q., Li, H.B., Chen, S.Y., 2003. Ultrahigh pressure eclogites of the north Qaidam and Altun mountains, NW China and their protoliths. Earth Science Frontiers 10, 291–314. in Chinese with English abstract.

Yang, J.S., Liu, F.L., Wu, C.L., Xu, Z.Q., Shi, R.D., Chen, S.Y., 2005. Two ultrahigh-pressure metamorphic events recognized in the Central Orogenic Belt of China: evidence from the U-Pb dating of coesite-bearing zircons. International Geology Review 47, 327–343.

Zhang, J.X., Zhang, Z.M., Xu, Z.Q., Yang, J.S., Cui, J.W., 2001. Petrology and geochronology of eclogites from the western segment of the Altyn Tagh, northwestern China. Lithos 56, 189–208.

Zhang, L.F., Ellis, D.J., Jiang, W.B., 2002a. Ultrahigh pressure metamorphism in western Tianshan, China, part I: evidences from the inclusion of coesite pseudomorphs in garnet and quartz exsolution lamellae in omphacite in eclogites. American Mineralogist 87, 853–860.

Zhang, L.F., Ellis, D., Williams, S., Jiang, W.B., 2002b. Ultrahigh pressure metamorphism in western Tianshan, China, part II: evidence from magnesite in eclogite. American Mineralogist 87, 861–866.

Zhang, L.F., Ellis, David J., Arculous, Richard J., Jiang, W.B., Wei, C., 2003. Ultradeep subduction of carbonates to the mantle: evidence from the carbonate reaction of magnesite + calcite (aragonite) = dolomite in metapelites from western Tianshan, China. Journal of Metamorphic Geology 21, 523–529.

Zhang, G.B., Song, S.G., Zhang, L.F., Niu, Y.L., Shu, G.M., 2005a. Ophiolite-type mantle peridotite from Shaliuhe, North Qaidam UHPM belt, NW China and its tectonic implications. Acta Petrologica Sinica 21 (4), 1049–1058. in Chinese with English abstract.

Zhang, J.X., Yang, J.S., Mattinson, C.G., Xu, Z.Q., Meng, F.C., Shi, R.D., 2005b. Two contrasting eclogite cooling histories, North Qaidam HP/UHP terrane, western China: Petrological and isotopic constraints. Lithos 84, 51–76.

Zhang, L.F., Ai, Y.L., Song, S.G., Song, B., Rubatto, D., Williams, S., Liou, J.G., Ellis, D., 2007. Triassic collision of Western Tianshan orogenic belt, China: evidences from SHRIMP U-Pb dating of zircon from eclogitic rocks. Lithos 96, 266–280.

Zhang, G.B., Song, S.G., Zhang, L.F., Niu, Y.L., 2008. The subducted oceanic crust within continental-type UHP metamorphic belt in the North Qaidam, NW China: evidence from petrology, geochemistry and geochronology. Lithos 104, 99–118.

Zheng, Y.F., Fu, B., Gong, B., Li, L., 2003. Stable isotope geochemistry of ultrahigh-pressure metamorphic rocks from the Dabie-Sulu orogen in China: implications for geodynamics and fluid regime. Earth Science Review 62, 105–161.

Zhang, J.X., Meng, F.C., Li, J.P., Mattinson, C.G., 2009. Coesite in eclogite from the North Qaidam and its implications. Chinese Science Bulletin, in press.